

<https://doi.org/10.1038/s41612-025-01211-9>

Ocean-atmosphere coupling enhances Eurasian cooling in response to historical Barents-Kara sea-ice loss



Mian Xu¹, Shichang Kang^{1,2}✉, James A. Screen³, Alexandre Audette⁴, Wenshou Tian⁵, Jiankai Zhang⁵, Hao Yu³ & Han Zhang⁶

The potential for Arctic sea-ice loss, particularly in the Barents-Kara Seas, to induce Eurasian winter cooling remains contentious. Despite a significant correlation between Barents-Kara-Seas sea-ice loss and Eurasian winter cooling in observations, modeling studies suggest minimal causal influence. Through constraining Barents-Kara-Seas sea-ice to different states in ocean-atmosphere-coupled simulations, here we show that ocean-atmosphere coupling enhances the Eurasian cooling induced by historical sea-ice loss, though still weaker than observed, likely due to internal variability and confounding factors. Historical sea-ice loss induces stronger and deeper Arctic warming with ocean-atmosphere coupling than without, associated with a strengthened Siberian High and East Asian Trough, which promotes Eurasian cooling. However, ocean-atmosphere coupling has little influence on the Eurasian cooling response to projected end-of-the-twenty-first-century sea-ice loss. The Eurasian temperature response to historical sea-ice loss is dominated by dynamically-induced cooling, whereas strong thermodynamical warming masks dynamically-induced cooling in response to far-future sea-ice loss.

The possible connection between Arctic sea-ice loss, especially over the Barents-Kara Seas (BKS), and winter cold extremes over mid-latitude Eurasia remains contentious, with conflicting lines of evidence^{1–4}. Despite observed significant correlation between the reduced BKS sea-ice and cold Eurasian winters, many modeling studies reveal contradictory results. While some model experiments suggest a significant winter Eurasian cooling^{2,5}, many others lack a significant cooling signal, or even simulate significant warming^{6–8}. Even those model experiments supporting a causal linkage between BKS sea-ice loss and Eurasian cooling suggest the cooling response is weak compared to internal variability and that the causal effect is weaker than implied from the observed statistical relationship^{9–11}. Therefore, many studies argued that internal variability, instead of sea-ice decline, plays a major role in the recent frequent occurrence of cold outbreaks over Eurasia, while BKS sea-ice loss only makes a minimal contribution^{3,12}. However, most of the above-mentioned modeling studies are based on atmosphere-only simulations, neglecting the potential contribution of ocean-atmosphere coupling that could enhance the response to sea-ice loss^{13,14}.

The importance of ocean-atmosphere coupling for the atmospheric response to far-future pan-Arctic sea-ice loss has been examined, using different approaches to constrain sea-ice in a coupled model framework. Through adding an additional heat flux to melt sea ice towards a reference state (“ghost-flux forcing” method), Deser et al.^{13,14} and some other studies^{15,16} found that ocean-atmosphere coupling plays a critical role in extending the influence of Arctic sea-ice loss to the tropics and even into the Southern Hemisphere. However, Deser et al.¹⁴ found in their coupled simulations a weaker Eurasian cooling response to projected future sea-ice loss at the end of the twenty-first century, compared to that in uncoupled simulations. They hypothesized that a relatively greater enhancement of thermodynamical warming, stemming from the advection of air warmed by sea-ice loss, overwhelms dynamical cooling, arising from atmospheric circulation changes. Studies using other methods—specifically, through altering the surface albedo (“albedo forcing” method) and nudging sea-ice concentration (SIC) and volume (“direct nudging” method)—also suggest little influence of ocean-atmosphere coupling on the Eurasian cooling in response to projected sea-ice loss^{3,12,17–20}.

¹Key Laboratory of Cryospheric Science and Frozen Soil Engineering, Northwest Institute of Eco-Environment and Resources, Chinese Academy of Sciences, Lanzhou, China. ²University of Chinese Academy of Sciences, Beijing, China. ³Department of Mathematics and Statistics, University of Exeter, Exeter, UK.

⁴Department of Earth and Planetary Sciences, University of California, Santa Cruz, Santa Cruz, CA, USA. ⁵College of Atmospheric Sciences, Lanzhou University, Lanzhou, China. ⁶School of Atmospheric Sciences, and Key Laboratory of Tropical Atmosphere-Ocean System, Ministry of Education, Sun Yat-Sen University, Zhuhai, China. ✉e-mail: shichang.kang@lzb.ac.cn

The aforementioned studies examining the role of ocean-atmosphere coupling all considered the response to far-future pan-Arctic sea-ice loss under a high greenhouse gas emissions scenario. However, the nature of the response to sea-ice loss could change over time, dependent on the magnitude and spatial pattern of sea-ice loss. For example, there is evidence that the Eurasian cooling response is greater for near-future than for far-future sea-ice loss⁵, or is greater in response to moderate than large sea-ice loss²¹. Over Eurasia, the thermodynamic warming response might be relatively more important than the dynamical cooling response into the future or as the magnitude of sea-ice loss increases. Thus, the importance of ocean-atmosphere coupling to Eurasian cooling may also depend on the magnitude and spatial pattern of sea-ice loss. Here, we find that ocean-atmosphere coupling enhances the Eurasian cooling induced by historical sea-ice loss due to a stronger large-scale circulation response. However, ocean-atmosphere coupling has little influence on the Eurasian cooling response to projected end-of-the-twenty-first-century sea-ice loss, in which thermodynamical warming masks dynamically-induced cooling.

Results

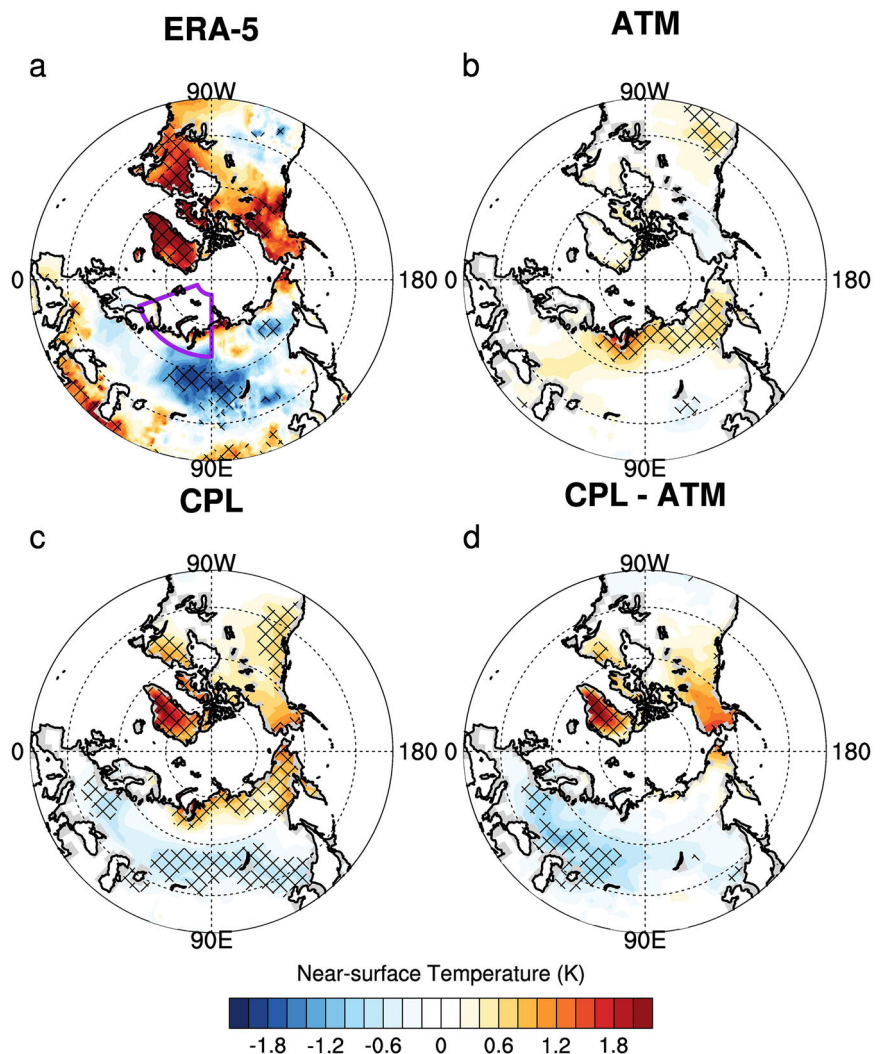
Ocean-atmosphere coupling enhances Eurasian cooling response to historical sea-ice loss

To identify the role of ocean-atmosphere coupling in winter Eurasian cooling induced by BKS sea-ice loss, we performed two sets of CESM simulations. One set is atmosphere-only with prescribed historical BKS high- and low-SIC conditions (atm_hi and atm_lo), and the other is coupled

to a full ocean model, with BKS sea-ice constrained towards the above-mentioned high and low states using a state-of-the-art sea-ice nudging method²² (cpl_hi and cpl_lo). For more details on the simulation scheme, please refer to the “Methods” section. Moreover, both our results (Supplementary Fig. 1) and some previous studies^{10,23} reveal a greater Eurasian cooling signal induced by BKS sea-ice loss in late winter (January–February) than in early winter (November–December). Therefore, in the following, we mainly focus on the late-winter Eurasian cooling.

Figure 1a clearly shows that there are strong late-winter cold anomalies observed over mid-latitude Eurasia, associated with historical early-winter BKS sea-ice loss. It should be noted, of course, that this does not necessarily indicate causality, which requires model simulations to elucidate. In our atmosphere-only simulations, there are no significant cold anomalies in response to BKS sea-ice reduction (Fig. 1b), consistent with many studies based on atmosphere-only experiments that found a minimal role of sea-ice loss^{7,8}. On the contrary, in coupled simulations, strong and widespread Eurasian cooling appears, spanning from Eastern Europe to Eastern Siberia (Fig. 1c, d), albeit still notably weaker than the observed regression, especially over central Siberia. This suggests that ocean-atmosphere coupling enhances the Eurasian cooling response to historical BKS sea-ice loss, bringing it closer to the observed estimate. However, the estimate of the forced response in the coupled simulations remains less than observed, likely due to internal variability and confounding factors that lead to an overestimation of the forced response to sea-ice loss derived from observed statistical relationships¹¹.

Fig. 1 | Observed and simulated late-winter Eurasian cooling response to historical sea-ice loss.
a Regression map of early-winter (November–December) BKS sea-ice concentration (SIC) against late-winter (January–February) T_{2m} during 1979–2019, scaled by the early-winter BKS SIC difference between BKS low- and high-SIC years (K). **b** 200-year simulated differences of late-winter T_{2m} between the atmosphere-only historical BKS low- and high-SIC simulations (atm_lo minus atm_hi). **c** The same as (b), but for the coupled historical BKS low- and high-SIC simulations (cpl_lo minus cpl_hi). **d** The differences between c and b (c minus b). Purple box in **a** denotes the BKS region (10° – 120° E, 45° – 60° N). Cross-hatching denotes the statistical significance at the 95% confidence level according to bootstrap resampling.



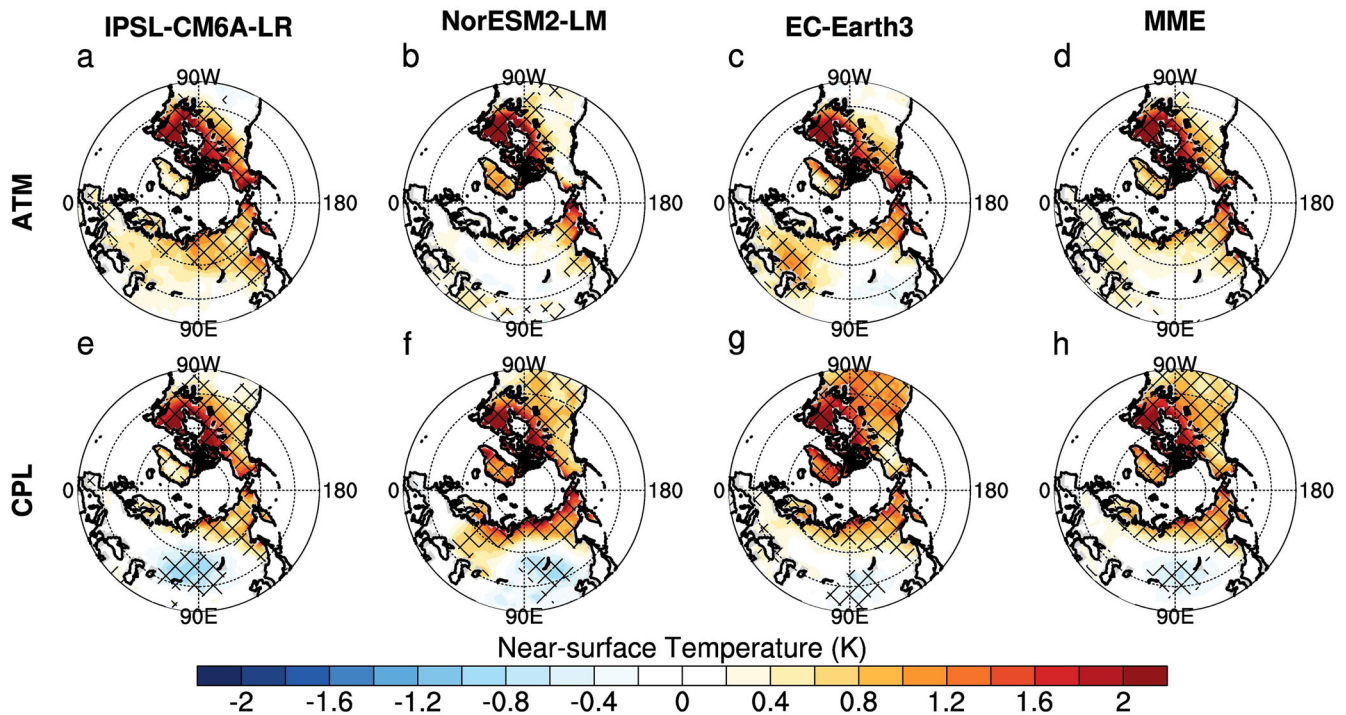


Fig. 2 | Simulated Eurasian temperature responses to sea-ice loss in PAMIP simulations. Differences of late-winter (January–February) T_{2m} between PAMIP pdSST-futArcSIC and pdSST-pdSIC runs, derived from **a** IPSL-CM6A-LR, **b** NorESM2-LM, **c** EC-Earth3, and **d** multi-model ensemble mean (MME). **e–h** are

the same as (a–d), but for differences between pa-futArcSIC-ext and pa-pdSIC-ext runs. Cross-hatching denotes the statistical significance at the 95% confidence level according to bootstrap resampling.

To check whether the above-mentioned results are model-dependent, the multi-model atmosphere-only and long-coupled simulations (100-year simulation) provided by the Polar Amplification Model Intercomparison Project (PAMIP)²⁴ are also analyzed (Fig. 2). Note that we used PAMIP simulations driven by pan-Arctic, rather than BKS, sea-ice loss, as the PAMIP project does not provide coupled simulations driven by the BKS sea-ice loss alone. However, in winter, the sea-ice changes in these experiments are largest over the BKS region²⁴, which further justifies their use here. Although these PAMIP simulations compare present-day and near-future sea-ice states, the prescribed and constrained sea-ice loss is more similar to that in our historical experiments than in our far-future experiments (Supplementary Fig. 2b–d). The PAMIP multi-model ensemble (MME) reveals a similar result, with significant Eurasian cooling in the long-coupled simulations (Fig. 2h), but no cooling in the atmosphere-only simulations (Fig. 2d). The three individual models in the PAMIP ensemble also all show a similar dependence on ocean-atmosphere coupling (Fig. 2a–c, e–g). The PAMIP also provides ensembles of short (1 year)-coupled simulations. It is notable that these short-coupled simulations lack significant Eurasian cooling²⁵, suggesting the necessity to include both fast sea-air interaction and slow ocean dynamics; timescale of the latter depends on ocean depth, that is, around 60–100 years for shallow ocean (above ~1000 m), while up to 1000 years or more for a deeper ocean^{25–27}.

Masked Eurasian cooling response to far-future sea-ice loss

Deser et al.^{13,14} found a weaker Eurasian cooling in the coupled simulations compared to atmosphere-only in response to far-future pan-Arctic sea-ice loss and hypothesized that ocean-atmosphere coupling enhanced thermodynamical warming relatively more than dynamical cooling. However, note that these studies arguing ocean-atmosphere coupling damps the sea-ice-induced Eurasian cooling focus on sea-ice loss of a much larger amplitude, compared with what we presented above. To reconcile our finding of a stronger cooling in the coupled experiments with the contradictory results from Deser et al.^{13,14}, we performed additional experiments representing BKS sea-ice loss at the end of the twenty-first century under a high

greenhouse gas emission scenario, more comparable to the experiments in Deser et al.^{13,14}. In the case of far-future sea-ice loss, Eurasian cooling is weaker in the coupled than atmosphere-only experiments, consistent with Deser et al.¹³ (Fig. 3), and weaker than that in historical sea-ice coupled runs (Fig. 1c). The Eurasian temperature response to sea-ice loss can be understood as the balance between thermodynamical warming, stemming from the advection of air warmed by sea-ice loss, and dynamical cooling, arising from atmospheric circulation changes (like East Asian Trough²⁸, Ural blocking^{29,30}, Siberian High³¹, and so on). We further decompose the T_{2m} response into the contribution of dynamical and thermodynamical processes, following a simple method of Zheng et al.³² (see “Methods”). In this method, the part of Eurasian cooling correlated with 500-hPa BKS geopotential height variability is regarded as contributed by large-scale circulation changes, i.e., “dynamical” process, with the residual attributed to “thermodynamical” process, including many other factors, like warm/cold air advection. However, this method is only approximate, since not all dynamical aspects are included in the “dynamical” term. It can be found in Fig. 4a, b that the Eurasian cooling induced by historical sea-ice loss is mainly contributed by the dynamical cooling, whereas the signal of thermodynamic process is relatively weak. In response to far-future sea-ice loss, which is of larger magnitude, both thermodynamical warming and dynamical cooling are enhanced (Fig. 4c, d), with the former largely canceling the latter and leading to a weaker Eurasian cooling in the coupled simulations (Fig. 3b). This could be due to that despite the strengthened atmospheric circulation adjustments (discussed in the following section) and the subsequent intensified Eurasian dynamical cooling (Fig. 4c), a much stronger and more widespread polar warming in response to far-future sea-ice loss (Supplementary Fig. 3) is also favorable for the warm air advection into the continent (Fig. 4d), which eventually cancels out the Eurasian cooling signal.

How ocean-atmosphere coupling amplifies Eurasian cooling response to historical sea-ice loss

We now return to the response to historical sea-ice loss and seek to explain why ocean-atmosphere coupling enhances the Eurasian cooling response.

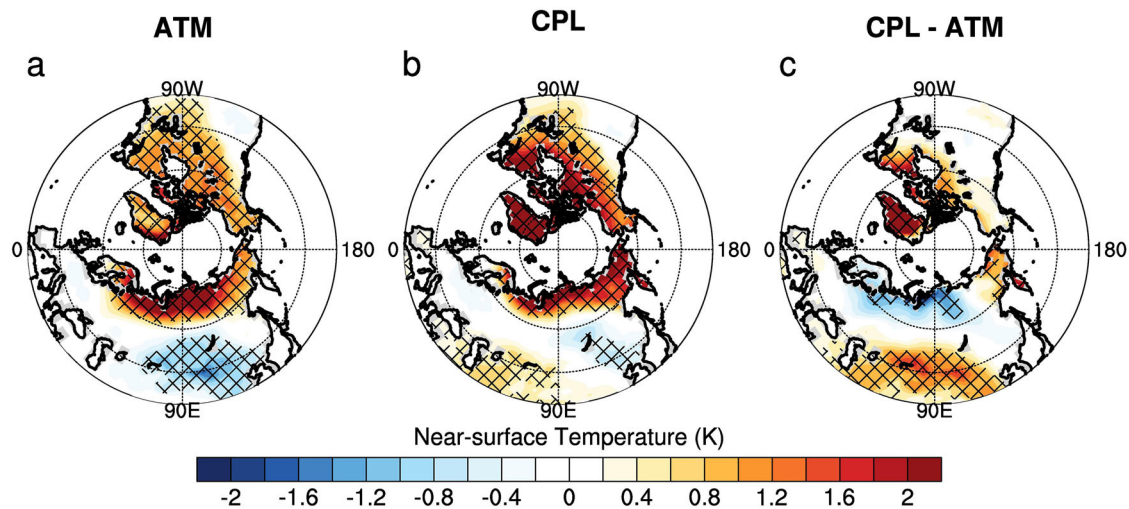


Fig. 3 | Eurasian temperature responses to future sea-ice loss. **a** 200-year simulated differences of late-winter (January–February) T_{2m} between the atmosphere-only BKS future and present-day SIC simulations (atm_fut minus atm_pd). **b** the same as **(a)**, but for the coupled BKS future and present-day SIC simulations (cpl_fut minus cpl_pd). **c** The differences between **b** and **a** (**b** minus **a**). Cross-hatching denotes the statistical significance at the 95% confidence level according to bootstrap resampling.

Fig. 4 | Decomposition of dynamical and thermodynamical contributions to Eurasian cooling. Contributions of **a** dynamical and **b** thermodynamical processes, respectively, to the 200-year simulated differences of late-winter (January–February) T_{2m} (K) between the coupled BKS historical low- and high-SIC simulations (cpl_lo and cpl_hi). **c**, **d** are the same as **(a)**, **(b)**, but for the differences between the coupled BKS future and present-day SIC simulations (cpl_fut and cpl_pd). Most of the results pass the 95%-level significance test, and therefore, the statistical significance tests are not shown for visual clarity.

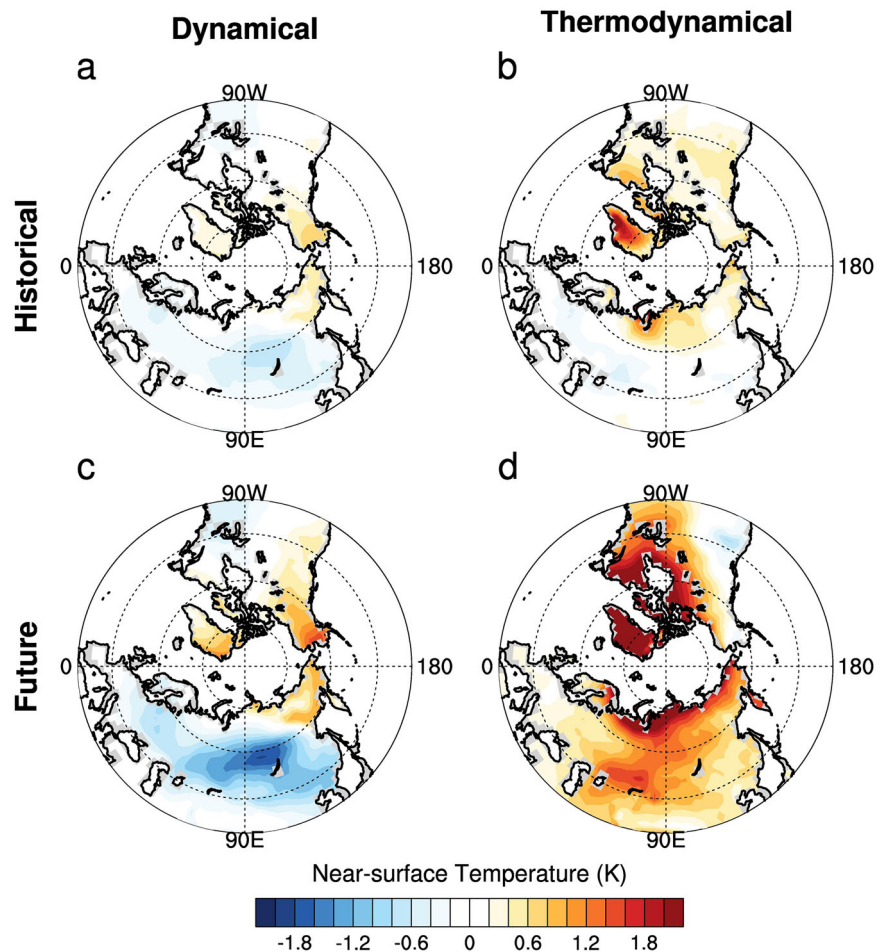


Figure 5 shows the differences of SIC, SST, and surface upward turbulent heat flux (THF) between low and high BKS SIC scenarios, derived from observations and model simulations. In the observed composite differences, there are negative SIC anomalies over the Chukchi Sea and Greenland Sea, in addition to the BKS (Fig. 5a). Moreover, there are warmer SSTs over the

BKS, Bering–Chukchi Seas, the North Atlantic, and North Pacific (Fig. 5e), resulting in the enhanced surface upward THF over these regions (Fig. 5i). In the atmosphere-only simulations, SIC, SST (prescribed), and THF (simulated) anomalies are confined to the BKS (Fig. 5b, f, j). With ocean–atmosphere coupling included, there is a weak signal of sea-ice loss over the

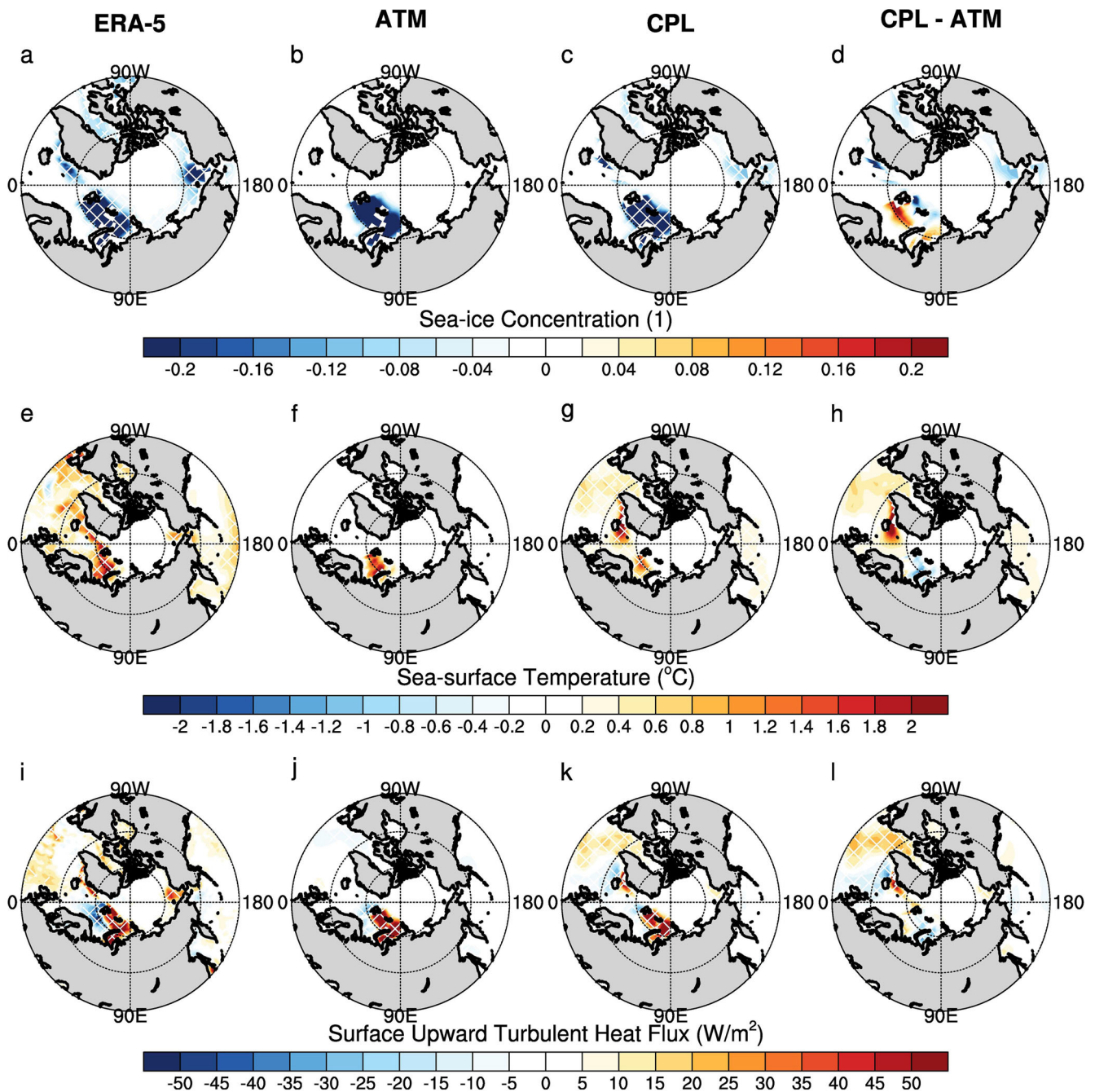


Fig. 5 | Atmospheric lower boundary response to historical sea-ice loss.

a Regression map of early-winter (November–December) BKS SIC against early-winter SIC during 1979–2019, scaled by the early-winter BKS SIC difference between BKS low- and high-SIC years (1). **b** Differences of the prescribed early-winter SIC between the atmosphere-only BKS historical low- and high-SIC simulations (atm_lo and atm_hi). **c** 200-year simulated differences of early-winter SIC between the coupled BKS historical low- and high-SIC simulations (cpl_lo and cpl_hi). **d** Differences between **c** and **b**. **e–h** are the same as (**a–d**), but for early-winter SST

(°C). **i** Regression map of early-winter BKS SIC against early-winter surface upward THF during 1979–2019, scaled by the early-winter BKS SIC difference between BKS low- and high-SIC years (W/m^2). **j** 200-year simulated differences of early-winter surface upward THF between the atmosphere-only BKS historical low- and high-SIC simulations (atm_lo minus atm_hi). **k** The same as (**j**), but for the coupled BKS historical low- and high-SIC simulations (cpl_lo minus cpl_hi). **l** The differences between **k** and **j** (**k** minus **j**). Cross-hatching denotes the statistical significance at the 95% confidence level according to bootstrap resampling.

Chukchi Sea and around Greenland (Fig. 5c, d) and SST warming over the North Atlantic (Fig. 5g, h), which are also seen in the observed composite difference, suggesting BKS sea-ice loss is partly responsible for these SIC and SST anomalies. Sea-ice loss around Greenland and North Atlantic SST warming could enhance the poleward heat and moisture transport, favorable for the vertical extension of Arctic warming^{33–35}, while Chukchi Sea sea-ice loss could also lead to Eurasian winter cooling^{36,37}.

Figure 6a–d shows the vertical extent of warming induced by BKS sea-ice loss in observations and simulations. Observed warming is clear throughout the polar troposphere, with two maxima: near the surface and in the upper troposphere (Fig. 6a). In the atmosphere-only simulations, Arctic warming is more confined to the lower troposphere, and the upper tropospheric maximum is absent. Consistent with some previous studies^{17,38}, deeper and stronger Arctic warming is simulated in the coupled experiments, more alike the observations. Blackport and Kushner³⁹ suggest that

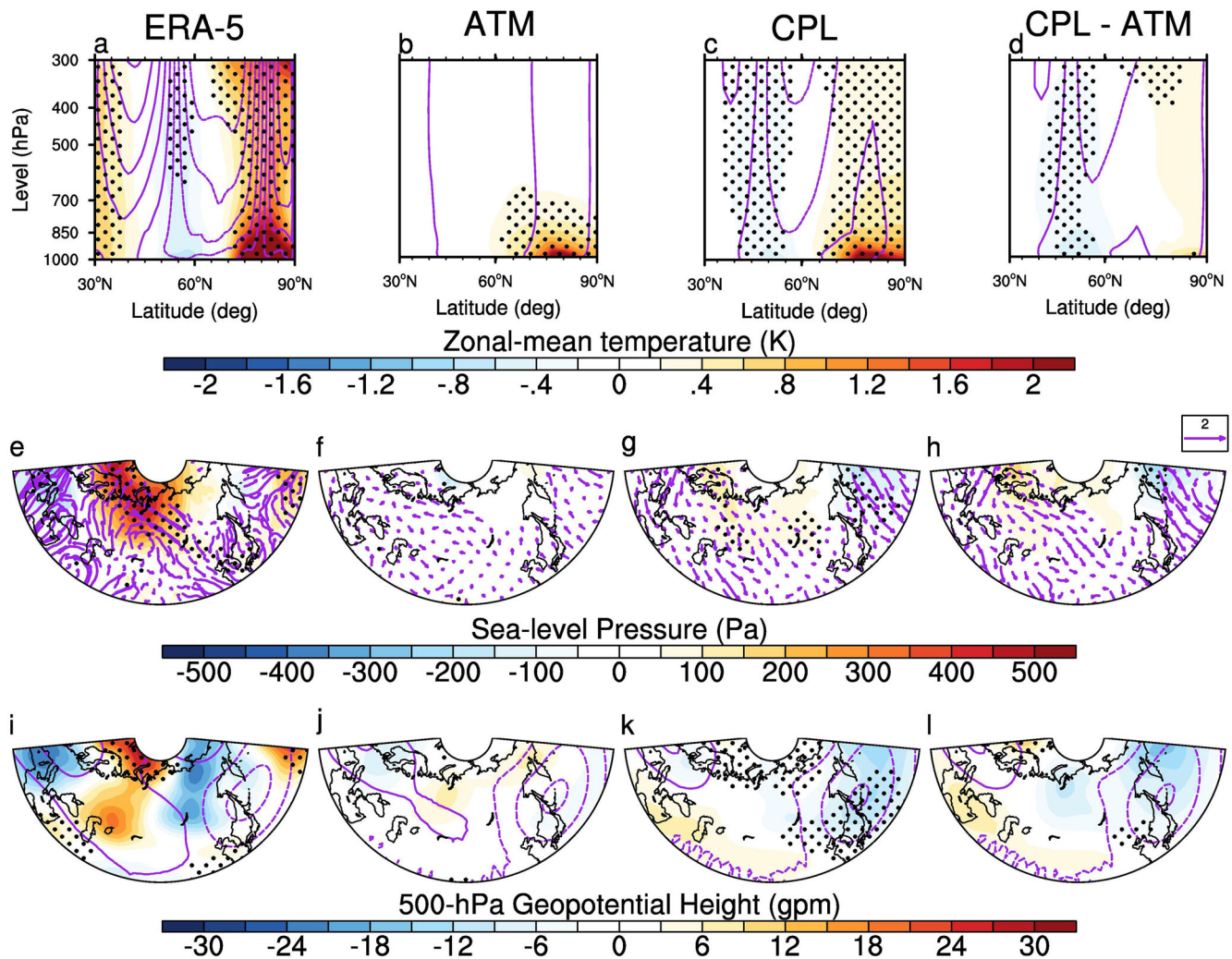


Fig. 6 | Large-scale circulation responses to historical sea-ice loss. **a** Regression map of early-winter (November–December) BKS SIC against late-winter (January–February) 0° – 150° E-mean zonal-mean air temperature (shading; K) and zonal wind (purple contours, with solid/dashed lines denoting positive/negative values; m s^{-1}) during 1979–2019, scaled by the early-winter BKS SIC difference between BKS low- and high-SIC years. **b** 200-year simulated differences of late-winter 0° – 150° E-mean zonal-mean air temperature (shading) and zonal wind (purple contours) between the atmosphere-only historical BKS low- and high-SIC simulations (atm_lo minus atm_hi). **c** The same as (**b**), but for the coupled historical

BKS low- and high-SIC simulations (cpl_lo minus cpl_hi). **d** The differences between **c** and **b** (c minus b). **e–h**, **i–l** are the same as (**a–d**), but for SLP (Pa; shading), 250-hPa Rossby wave flux ($\text{m}^2 \text{s}^{-2}$; purple vector) and 500-hPa geopotential (gpm; with zonal mean removed), respectively. Purple contours in (**i–l**) denote the climatology of **i** ERA-5 1979–2019 reanalysis, **j** atm_hi and **k**, **l** cpl_hi, respectively (with zonal mean removed; solid/dashed line denotes positive/negative values). Black stippling denotes the statistical significance at the 95% confidence level according to bootstrap resampling.

the extratropical ocean warming induced by Arctic sea-ice loss could play a critical role in the vertical extension of polar warming. We also found in our coupled simulations that BKS sea-ice loss could lead to the North Atlantic SST warming (Fig. 5g, h), which is favorable for the northward heat transport and the formation of this deep warming structure^{25–33,40}. However, it should be noted that coupled simulations still lack the upper tropospheric maximum. This implies that the observed polar upper tropospheric warming maximum is related to factors other than BKS sea-ice loss or, given its dependence on stratosphere-troposphere coupling⁴¹, it might suggest too weak stratosphere-troposphere coupling in the model simulations. Previous literature highlighted the importance of stratosphere-troposphere coupling in the Arctic-mid-latitude teleconnection. Specifically, Arctic sea-ice loss could amplify the sea-ice-loss-induced Eurasian winter cooling through modulating the SPV's intensity^{9,10}, position⁴² or shape^{43–45}. Figure 7 shows the responses of planetary-scale wave activity and zonal-mean wind to historical BKS sea-ice loss. Although observation implies this well-documented stratospheric pathway (Fig. 7a, d), there is no evidence that historical BKS sea-ice loss enhances the upward propagating waves and

weakens the stratospheric polar vortex in either the atmosphere-only or coupled simulations (Fig. 7b, c, e, f). The insignificant response of the stratospheric polar vortex in model simulations could be due to insufficient ensemble size^{20,46} or other aspects of this model and/or experimental design. Also note that despite the same model and similar experimental design, the atmosphere-only simulations in this study fail to reproduce the results reported in our previous studies^{10,41,47}. This could be partly due to the different simulation mean states between this and previous studies, like the SST climatology applied. Therefore, in this study, the stratospheric pathway could play a minimal role in the Eurasian cooling due to historical BKS sea-ice loss. In addition, it is worth noting that both atmosphere-only and coupled simulations driven by far-future sea-ice loss capture the signal of SPV weakening, with the latter stronger than the former (Fig. 8). This suggests the SPV response to BKS sea-ice loss could depend on the magnitude of sea-ice loss, consistent with Zhang et al.²¹. Previous works suggest that a deeper Arctic warming is more likely to stimulate a southeastward-propagating wave train, which subsequently modulates the mid-latitude large-scale circulation, like westerly jet, Ural blocking, and so on^{41,48–54}. Thus,

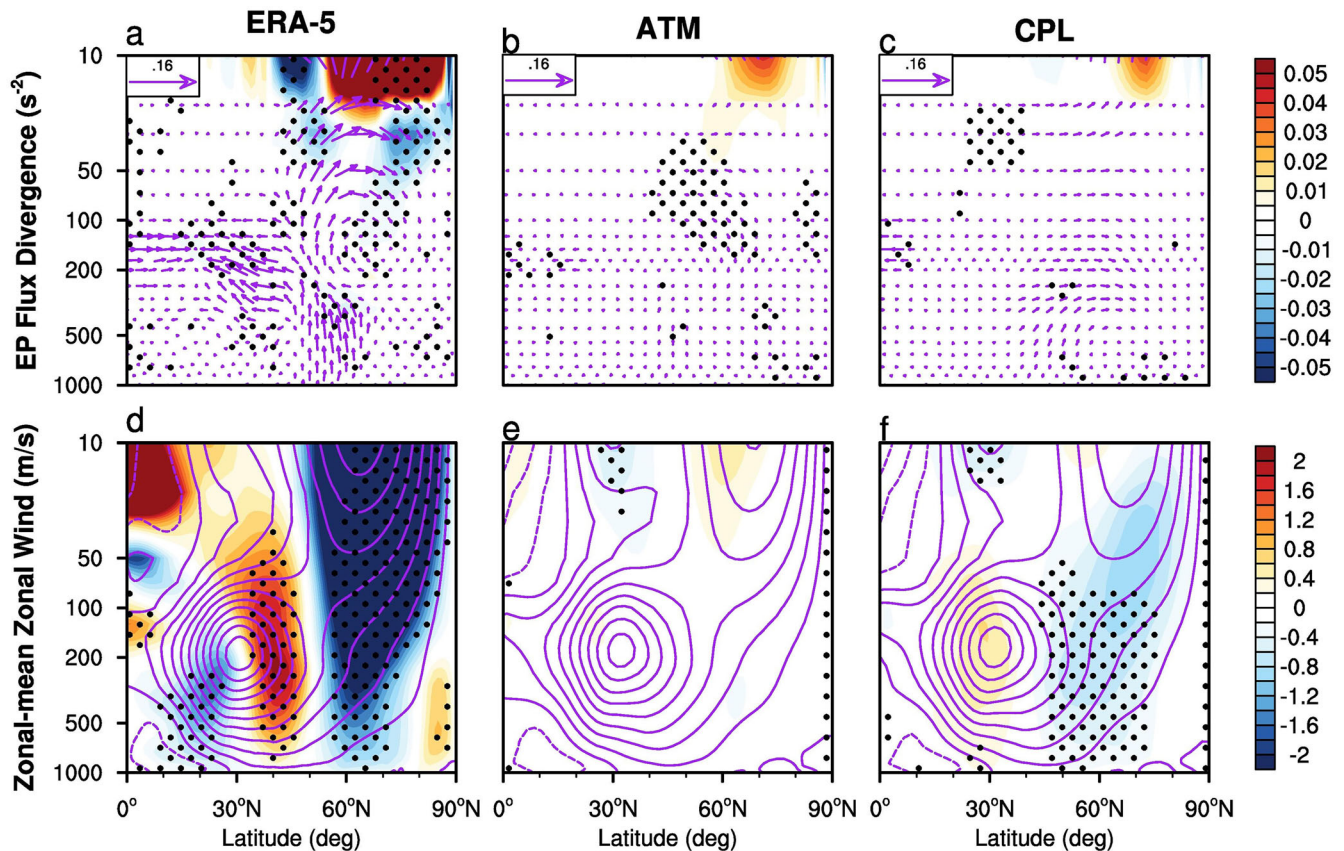


Fig. 7 | Stratospheric polar vortex response to historical sea-ice loss. **a** Wintertime (December–January–February) EP fluxes (purple arrows; scaled by air pressure; the vertical component is scaled by 10^4 and the meridional component is scaled by 10^6 ; m s^{-2}) of zonal wave 1–2 and their divergence (shading; scaled by air pressure; s^{-2}) regressed against early-winter BKS SIC, scaled by the early-winter BKS SIC difference between BKS low- and high-SIC years. **b** 200-year simulated differences of wintertime (December–January–February) EP fluxes (purple arrows; scaled by air pressure; the vertical component is scaled by 10^4 and the meridional component is scaled by 10^6 ; m s^{-2}) of zonal wave 1–2 and their divergence (shading; scaled by air

pressure; s^{-2}) between the atmosphere-only historical BKS low- and high-SIC simulations (atm_lo minus atm_hi). **c** the same as (**b**), but for the coupled historical BKS low- and high-SIC simulations (cpl_lo minus cpl_hi). **d–f** are the same as (**a–c**), but for wintertime zonal-mean zonal wind (m/s). Purple contours denote the climatological mid-winter zonal-mean zonal wind derived from **d** ERA-5 reanalysis during 1979–2019, **e** atm_hi and **f** cpl_hi simulations, with solid/dashed lines denoting positive/negative values. Black stippling denotes the statistical significance at the 95% confidence level according to bootstrap resampling.

we could expect a stronger response of large-scale atmospheric circulation in the coupled than atmosphere-only simulations.

Notably, both observation (Fig. 6a) and our coupled simulations (Fig. 6c) capture the signal of westerly jet deceleration over the Eurasian sector (0° – 150°E) by historical BKS sea-ice loss, with the latter weaker than the former. Instead, there is no significant signal of westerly deceleration in the atmosphere-only simulations (Fig. 6b, d), confirming Arctic deep warming is more likely to decelerate the westerly jet stream than a shallow warming. This creates a favorable environment for the southeastward propagation of Rossby waves⁵⁵ from the BKS region to north Eurasia (Fig. 6e, g), strengthening the high-pressure anomalies over northern Eurasia, implying a strengthening of the Siberian High. The Siberian High modulates Eurasian winter weather and climate, with a stronger Siberian High favorable for anomalous cooling^{56,57}. In addition, there are also southward propagating Rossby waves over the North Pacific in the coupled simulations, leading to a deepening of the Aleutian Low (Fig. 6g), which could also induce Eurasian cooling⁵⁸. However, a deeper Aleutian Low is not found in observation (Fig. 6e), possibly masked by other signals. As there is only a shallow warming, the above-mentioned signals of southeastward-propagating Rossby wave, strengthened Siberian High, and deepened Aleutian Low are not found in the atmosphere-only simulations (Fig. 6j, l), consistent with the absence of Eurasian cooling in these experiments. At 500-hPa, the coupled simulations show negative geopotential

height anomalies over East Asia (Fig. 6k), implying a deepening of the East Asian Trough, which is favorable for Eurasian cold anomalies^{47,59}. A similar feature but lacking significance is presented in the observations, but is absent in the atmosphere-only simulations (Fig. 6i, j). Although Ural blocking is a key part in the Arctic-mid-latitude teleconnection^{29,30}, no significant increase of its frequency is found in our model simulations driven by historical BKS sea-ice loss (Supplementary Fig. 4), implying its relatively minor role in this case. It should be noted that the above-mentioned mechanism could work in both directions: a stronger Siberian High may also favor deeper Arctic warming⁶⁰. However, additional simulations beyond the scope of this study would be required to separate these influences. While we argue that deeper Arctic warming is a potential cause for stronger Eurasian cooling, supported by observed and modeled evidence^{48,49}, further investigation is warranted.

Discussion

Previous studies have suggested that ocean-atmosphere coupling damps, or has little effect on, the Eurasian cooling response to sea-ice loss. Whilst we were able to replicate their results for the response to far-future sea-ice loss, we reached an opposite conclusion in the context of historical sea-ice loss. We find that ocean-atmosphere coupling enhances the late-winter Eurasian cooling response to historical BKS sea-ice loss. The simulated cooling in the coupled runs is

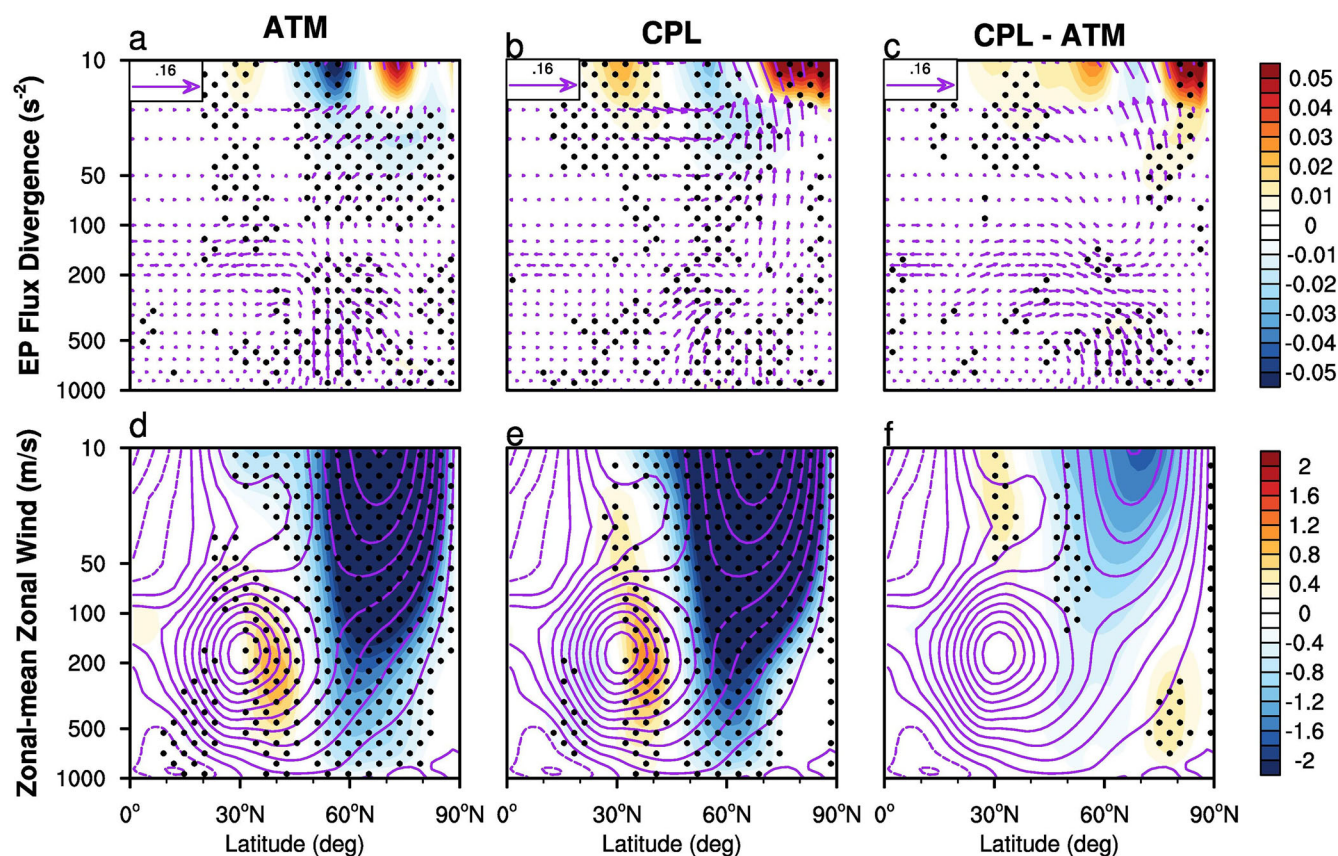


Fig. 8 | Stratospheric polar vortex response to future sea-ice loss. **a** 200-year simulated differences of wintertime (December–January–February) EP fluxes (purple arrows; scaled by air pressure; the vertical component is scaled by 10^4 and the meridional component is scaled by 10^6 ; m s^{-2}) of zonal wave 1–2 and their divergence (shading; scaled by air pressure; s^{-2}) between the atmosphere-only BKS future and present-day SIC simulations (atm_fut minus atm_pd). **b** The same as **(a)**, but for the coupled BKS future and present-day SIC simulations (cpl_fut minus cpl_pd). **c** The

differences between **b** and **a** (**b** minus **a**). **d–f** are the same as **(a–c)**, but for wintertime zonal-mean zonal wind (m/s). Purple contours in **(d–f)** denote the climatological wintertime zonal-mean zonal wind derived from **d** atm_pd and **e**, **f** cpl_pd simulations, with solid/dashed lines denoting positive/negative values. Black stippling denotes the statistical significance at the 95% confidence level according to bootstrap resampling.

still weaker than observed, likely due to internal variability and confounding factors that contaminate estimates of the forced response to sea-ice loss derived from observations¹¹. In the coupled simulations, the resultant Arctic warming is deeper and stronger than without coupling, and this deeper warming stimulates southeastward-propagating Rossby waves, further strengthening the Siberian High and East Asian Trough, both of which are favorable for Eurasian cooling. Moreover, our results also imply there could be a point in time when Arctic sea-ice loss ceases to have a cooling effect over Eurasia, which warrants further detailed study.

Although the inclusion of ocean coupling increases the modeled estimate of the forced response to BKS sea-ice loss, bringing it closer to observations, we need to be mindful that it could be the wrong mechanisms. Concerns have been raised that nudging methods artificially add heat to the climate system and may overestimate the response to sea-ice loss^{61–63}. Although the hybrid sea-ice nudging method used here is arguably less prone to this problem than the original “ghost-flux” method, it still introduces artificial heat into the model and therefore could induce spurious signals^{62,63}. It is possible that the stronger responses in the coupled simulations, compared to uncoupled, are, at least partly, a spurious effect of the nudging technique, rather than a genuine effect of ocean-atmosphere coupling; although we note that the separation of “spurious” and “genuine” effects is open to interpretation (e.g., whether sea-ice loss is a sufficient or necessary causal driver). Therefore, further study is required in the future to reduce the “spurious” effect of this hybrid sea-ice nudging method as much as possible.

Methods

Reanalysis

Daily- and monthly-mean atmospheric fields during 1979–2020 are derived from the ECMWF ERA-5 reanalysis dataset, with a horizontal resolution of $1^\circ \times 1^\circ$ ⁶⁴. Monthly SST, SIC, and thickness (SIT) are derived from the Pan-Arctic Ice Ocean Modeling and Assimilation System (PIOMAS), which assimilates satellite SIC and SST observations⁶⁵. PIOMAS has a horizontal resolution of 276×360 (latitude \times longitude).

Definition of BKS high- and low-SIC years

The geographical extent of the BKS region is $20^\circ\text{--}90^\circ\text{E}$, $65^\circ\text{--}85^\circ\text{N}$ (purple box in Fig. 1a). Winter is defined as December–January–February mean, with early- and late-winter defined as November–December and January–February mean, respectively. The BKS high- and low-SIC years are selected based on the de-trended time series of PIOMAS 1979–2019 early-winter BKS SIC, using ± 1 standard deviation as the criterion. 1988, 1998, 2002, 2003, 2014, and 2019 are selected as the BKS high-SIC years, while 1979, 1984, 2009, 2012, and 2016 for the low-SIC years (Supplementary Fig. 2a). The observational analysis and SST/SIC/SIT boundary conditions for the model simulations are based on these selected years. In this study the sea-ice related signals from observations are estimated according to the following steps⁴¹: firstly, regress the atmospheric fields (near-surface temperature, sea-level pressure and so on) upon the early-winter BKS SIC time series; then, multiply the obtained regression maps by the composited difference of early-winter BKS SIC between its low and high years (-0.20 in this case; Supplementary Fig. 2b). Compared with directly compositing

differences between BKS low- and high-SIC years, this method takes into consideration the whole sea-ice time series and its co-variability with atmospheric circulation. However, it should be noted that both methods include signals from other external forcings.

Decomposition of dynamical cooling and thermodynamical warming

The method proposed by Zheng et al.³² is applied to estimate the contributions of dynamical and thermodynamical processes in the Eurasian temperature response to sea-ice loss. Firstly, the 200-year simulated T_{2m} response to sea-ice loss ($T_{2m_{BKS}}$) is randomly resampled 10,000 times, with a subset size of 100 years. Then, the response of 500-hPa geopotential height over the BKS ($Z500_{BKS}$) is also resampled in the same way. Zheng et al.³² found that $Z500_{BKS}$ could well represent the tropospheric circulation response to BKS sea-ice loss and is highly correlated with the sea-ice-loss-induced Eurasian T_{2m} anomalies. Lastly, the T_{2m} responses are regressed upon the $Z500_{BKS}$ responses based on these 10,000 100-year subsamples (Eq. 1). In Eq. 1, a and b denote the regression coefficient and residual term, respectively. The two terms on the right-hand side of Eq. (1) approximate the dynamical and thermodynamical contributions.

$$T_{2m_{BKS}} = a * Z500_{BKS} + b \quad (1)$$

E-P flux calculation

Eliassen-Palm flux (EP flux) is calculated using the following equations⁶⁶:

$$F_{\phi} = \rho_0 a \cos \phi (\bar{u}_z \bar{v}'\theta' / \bar{\theta}_z - \bar{v}'u') \quad (2)$$

$$F_z = \rho_0 a \cos \phi \{ [f - (a \cos \phi)^{-1} (\bar{u} \cos \phi)_{\phi} \bar{v}'\theta' / \bar{\theta}_z - \bar{w}'u'] \} \quad (3)$$

$$D_F = \frac{\nabla \cdot \vec{F}}{\rho_0 a \cos \phi} = \frac{(a \cos \phi)^{-1} \frac{\partial}{\partial \phi} (F_{\phi} \cos \phi) + \frac{\partial F_z}{\partial z}}{\rho_0 a \cos \phi} \quad (4)$$

where F_{ϕ} , F_z and D_F denote the meridional and vertical components of EP flux and its divergence, u , v , w , ϕ , θ , a , f , z and ρ_0 denote zonal, meridional and vertical wind components, latitude, potential temperature, Earth's radius, Coriolis parameter, log pressure and air density. Overbars and primes represent zonal-mean and departure from zonal mean.

Takaya & Nakamura Rossby wave flux

According to Takaya & Nakamura⁵⁵, horizontal Rossby wave fluxes \vec{W} are calculated using the following equation:

$$\vec{W} = \frac{p \cos \phi}{2|\vec{U}|} \left(\frac{U}{a^2 \cos^2 \phi} \left[\left(\frac{\partial \psi'}{\partial \lambda} \right)^2 - \psi' \frac{\partial^2 \psi'}{\partial \lambda^2} \right] + \frac{V}{a^2 \cos \phi} \left[\frac{\partial \psi'}{\partial \lambda} \frac{\partial \psi'}{\partial \phi} - \psi' \frac{\partial^2 \psi'}{\partial \lambda \partial \phi} \right] \right) \quad (5)$$

where p , ϕ , λ , ψ , \vec{U} , U , V and a denote pressure/1000 hPa, latitude, longitude, stream function, horizontal wind velocity and its zonal and meridional component, and Earth's radius. Prime and $|\cdot|$ denote perturbation and norm of a vector.

Model description and simulation scheme

CESM1.2.0 model is used to perform the simulations. The atmosphere, sea-ice, and ocean components used in this study are the Whole Atmosphere Community Climate Model 4 with Specified Chemistry⁶⁷, Community Ice Code 4⁶⁸, and Parallel Ocean Program 2⁶⁹.

Two pairs of experiments are performed, with each pair including a simulation with high BKS SIC and a simulation with low BKS SIC, using the atmosphere-only (atm_hi and atm_lo) and coupled (cpl_hi and cpl_lo)

frameworks. In the atmosphere-only simulations, the SST/SIC conditions are prescribed using the above-mentioned composited BKS high- and low-SIC conditions, while the SST/SIC conditions in the remaining regions are fixed at year 2000 conditions. SIT is constant in the atmosphere-only simulations. In the coupled simulations, a new hybrid nudging method developed by Audette and Kushner²² is applied to nudge the SIC/SIT state towards the target values. In this method, SIC and SIT are nudged towards the target values using direct sea-ice nudging¹⁷ and ghost-flux nudging¹⁸, respectively, to better capture the partitioning between SIC and SIT. Moreover, additional freshwater flux and equivalent water mass from the sea-ice melting are added to the model to conserve the total water content. Audette and Kushner²² provide evidence that this method has advantages over the traditional ghost-flux method, by allowing for better control over the SIC/SIT partitioning while conserving total water conservation. In our study, sea-ice nudging is confined only in the BKS region, and the nudging time-scales for SIC and SIT are 3 h and 5 days, respectively, which is determined after testing and validation to minimize the differences between the simulated and reference sea ice states. It can be found from Supplementary Fig. 2b that coupled simulations well reproduce the seasonal cycle of historical BKS SIC loss.

In addition, another 2 pairs of CESM experiments are performed with BKS sea-ice loss of a larger magnitude. These simulations are driven by the BKS SIC/SIT conditions during the years 1980–1999 under a historical scenario and years 2080–2099 under the Shared Socioeconomic Pathway 5-8.5 (SSP585) scenario, derived from MME of 23 CMIP6 models. The full list of the used models is shown in Supplementary Table 1, and the composite seasonal cycle of BKS SIC differences between the two scenarios is shown in Supplementary Fig. 2d. Except for the BKS sea ice, all the remaining forcings are identical to the simulations driven by historical BKS sea-ice loss. The simulation time for atmosphere-only and coupled simulations is 203 and 260 years, respectively, and only the last 200 years are analyzed. Note that long-coupled simulations, rather than short-coupled runs in some relevant studies^{20,32}, are deliberately performed in this study to include both the signals of fast sea-air feedback and slow ocean dynamic processes. Supplementary Table 2 shows the simulation scheme of the above-mentioned experiments.

PAMIP multi-model ensemble

MME simulations from the PAMIP²⁴ are used to check whether our results are model-dependent and robust in a larger ensemble with better sampling of internal variability. The models used in PAMIP and their corresponding ensemble sizes are included in Supplementary Table 3. Note that in these PAMIP simulations, sea ice is perturbed across the whole Arctic, not just in the BKS. The PAMIP project also provides simulations driven by the BKS sea-ice loss alone, but no coupled simulations are performed with nudged BKS sea-ice. Therefore, we only used pan-Arctic sea-ice simulations from the PAMIP project. Four PAMIP experiments are used: pdSST-pdSIC, pdSST-futArcSIC, pa-pdSIC-ext, and pa-futArcSIC-ext. As atmosphere-only simulations, pdSST-pdSIC and pdSST-futArcSIC are prescribed with the climatological SIC and SST during 1979–2008 derived from the HadISST1 dataset⁷⁰, with Arctic SIC/SST in pdSST-futArcSIC prescribed to that projected at 2 °C global warming above preindustrial levels. Each member in pdSST-pdSIC and pdSST-futArcSIC starts from April 2000 and ends in May 2001, with the first 2 months discarded as model spin-up. To keep in accordance with our coupled simulations, the extended coupled simulations of pa-pdSIC-ext and pa-futArcSIC-ext are used. In these simulations, Arctic SIC and SIT are nudged towards the present-day and 2-degree-global-warming states, respectively, through direct nudging. We use output from three models: EC-Earth3, NorESM2-LM, and IPSL-CM6A-LR. Although a fourth model (CNRM-CM6-1) also participated in these experiments, it applied an albedo reduction, instead of direct nudging, that resulted in more sea-ice loss than that prescribed in the atmosphere-only simulations (Supplementary Fig. 2c).

Statistical significance testing

Bootstrap resampling is applied to validate whether the composite analysis is statistically significant at the 95% level⁷¹. The two samples are resampled 1000 times with replacement, with a subset size of 10% of the total sample size.

Data availability

ERA-5 atmospheric reanalysis dataset is available from <https://cds.climate.copernicus.eu/cdsapp#!/dataset/reanalysis-era5-pressure-levels-monthly-means?tab=form>. PIOMAS sea-ice reanalysis dataset is available from https://psc.apl.uw.edu/research/projects/arctic-sea-ice-volume-anomaly/data/model_grid. CMIP6 and PAMIP simulations are available from <https://esgf-ui.ceda.ac.uk/cog/search/cmip6-ceda/>. CESM simulations are available from the corresponding author upon request.

Code availability

Source codes of the CESM1.2.0 model are available from <http://www.cesm.ucar.edu/models/cesm1.2/>. Modified source codes of the sea-ice hybrid nudging method are available from Audette⁷². Other codes used in this study are available from the corresponding author upon request.

Received: 6 June 2025; Accepted: 20 August 2025;

Published online: 29 August 2025

References

- Mori, M. et al. A reconciled estimate of the influence of Arctic sea-ice loss on recent Eurasian cooling. *Nat. Clim. Change* **9**, 123–129 (2019).
- Mori, M. et al. Robust Arctic sea-ice influence on the frequent Eurasian cold winters in past decades. *Nat. Geosci.* **7**, 869–873 (2014).
- McCusker, K. E., Fyfe, J. C. & Sigmond, M. Twenty-five winters of unexpected Eurasian cooling unlikely due to Arctic sea-ice loss. *Nat. Geosci.* **9**, 838–842 (2016).
- Screen, J. A. The missing Northern European winter cooling response to Arctic sea ice loss. *Nat. Commun.* **8**, 14603 (2017).
- Peings, Y. & Magnusdottir, G. Response of the wintertime Northern Hemisphere atmospheric circulation to current and projected Arctic sea ice decline: a numerical study with CAM5. *J. Clim.* **27**, 244–264 (2014).
- Chen, H. W., Zhang, F. & Alley, R. B. The robustness of midlatitude weather pattern changes due to Arctic sea ice loss. *J. Clim.* **29**, 7831–7849 (2016).
- Sun, L., Perlwitz, J. & Hoerling, M. What caused the recent “Warm Arctic, Cold Continents” trend pattern in winter temperatures?. *Geophys. Res. Lett.* **43**, 5345–5352 (2016).
- Ogawa, F. et al. Evaluating impacts of recent Arctic sea ice loss on the northern hemisphere winter climate change. *Geophys. Res. Lett.* **45**, 3255–3263 (2018).
- Zhang, P. et al. A stratospheric pathway linking a colder Siberia to Barents-Kara Sea sea ice loss. *Sci. Adv.* **4**, eaat6025 (2018).
- Xu, M. et al. Distinct tropospheric and stratospheric mechanisms linking historical Barents-Kara sea-ice loss and late winter Eurasian temperature variability. *Geophys. Res. Lett.* **48**, e2021GL095262 (2021b).
- Blackport, R. & Screen, J. A. Observed statistical connections overestimate the causal effects of Arctic sea ice changes on midlatitude winter climate. *J. Clim.* **34**, 3021–3038 (2021).
- Blackport, R. et al. Minimal influence of reduced Arctic sea ice on coincident cold winters in mid-latitudes. *Nat. Clim. Change* **9**, 697–704 (2019).
- Deser, C. et al. Does ocean coupling matter for the northern extratropical response to projected Arctic sea ice loss?. *Geophys. Res. Lett.* **43**, 2149–2157 (2016).
- Deser, C., Tomas, R. A. & Sun, L. The role of ocean–atmosphere coupling in the zonal-mean atmospheric response to Arctic sea ice loss. *J. Clim.* **28**, 2168–2186 (2015).
- Chemke, R., Polvani, L. M. & Deser, C. The effect of Arctic sea ice loss on the Hadley circulation. *Geophys. Res. Lett.* **46**, 963–972 (2019).
- England, M. R. et al. Tropical climate responses to projected Arctic and Antarctic sea-ice loss. *Nat. Geosci.* **13**, 275–281 (2020).
- Smith, D. M. et al. Atmospheric response to Arctic and Antarctic sea ice: The importance of ocean–atmosphere coupling and the background state. *J. Clim.* **30**, 4547–4565 (2017).
- Sun, L., Alexander, M. & Deser, C. Evolution of the global coupled climate response to Arctic sea ice loss during 1990–2090 and its contribution to climate change. *J. Clim.* **31**, 7823–7843 (2018).
- Dai, A. & Song, M. Little influence of Arctic amplification on mid-latitude climate. *Nat. Clim. Change* **10**, 231–237 (2020).
- Peings, Y., Labe, Z. M. & Magnusdottir, G. Are 100 ensemble members enough to capture the remote atmospheric response to +2 °C Arctic sea ice loss?. *J. Clim.* **34**, 3751–3769 (2021).
- Zhang, R. & Screen, J. A. Diverse Eurasian winter temperature responses to Barents-Kara sea ice anomalies of different magnitudes and seasonality. *Geophys. Res. Lett.* **48**, e2021GL092726 (2021).
- Audette, A. & Kushner, P. J. Simple hybrid sea ice nudging method for improving control over partitioning of sea ice concentration and thickness. *J. Adv. Model. Earth Syst.* **14**, e2022MS003180 (2022).
- Jang, Y., Jun, S., Son, S., Min, S. & Kug, J. Delayed impacts of Arctic sea-ice loss on Eurasian severe cold winters. *J. Geophys. Res. Atmos.* **126**, e2021JD035286 (2021).
- Smith, D. M. et al. The Polar Amplification Model Intercomparison Project (PAMIP) contribution to CMIP6: investigating the causes and consequences of polar amplification. *Geosci. Model Dev.* **12**, 1139–1164 (2019).
- Stouffer, R. Time scales of climate response. *J. Clim.* **17**, 209–217 (2004).
- Yang, H. & Zhu, J. Equilibrium thermal response timescale of global oceans. *Geophys. Res. Lett.* **38**, 14 (2011).
- Hogan, E. & Sriver, R. The effect of internal variability on ocean temperature adjustment in a low-resolution CESM initial condition ensemble. *J. Geophys. Res. Oceans* **124**, 1063–1073 (2019).
- Song, L. et al. Intraseasonal variation of the strength of the East Asian trough and its climatic impacts in boreal winter. *J. Clim.* **29**, 2557–2577 (2016).
- Luo, D. et al. Impact of Ural blocking on winter warm Arctic–cold Eurasian anomalies. Part I: Blocking-induced amplification. *J. Clim.* **29**, 3925–3947 (2016).
- Luo, D. et al. Impact of Ural blocking on winter warm Arctic–cold Eurasian anomalies. Part II: the link to the North Atlantic Oscillation. *J. Clim.* **29**, 3949–3971 (2016).
- Li, B. et al. Recent fall Eurasian cooling linked to North Pacific sea surface temperatures and a strengthening Siberian high. *Nat. Commun.* **11**, 5202 (2020).
- Zheng, C. et al. Diverse Eurasian temperature responses to Arctic sea ice loss in models due to varying balance between dynamic cooling and thermodynamic warming. *J. Clim.* **36**, 8347–8364 (2023).
- Ding, Q. et al. Tropical forcing of the recent rapid Arctic warming in northeastern Canada and Greenland. *Nature* **509**, 209–212 (2014).
- Hahn, L. et al. Contributions to polar amplification in CMIP5 and CMIP6 models. *Front. Earth Sci.* **9**, 710036 (2021).
- Henderson, G. et al. Local and remote atmospheric circulation drivers of Arctic change: a review. *Front. Earth Sci.* **9**, 709896 (2021).
- McKenna, C. et al. Arctic sea ice loss in different regions leads to contrasting Northern Hemisphere impacts. *Geophys. Res. Lett.* **45**, 945–954 (2018).
- Ding, S. & Wu, B. Linkage between autumn sea ice loss and ensuing spring Eurasian temperature. *Clim. Dyn.* **57**, 2793–2810 (2021).
- Screen, J. A. et al. Consistency and discrepancy in the atmospheric response to Arctic sea-ice loss across climate models. *Nat. Geosci.* **11**, 155–163 (2018).

39. Blackport, R. & Kushner, P. J. The role of extratropical ocean warming in the coupled climate response to Arctic sea ice loss. *J. Clim.* **31**, 9193–9206 (2018).
40. Audette, A. et al. Opposite responses of the dry and moist eddy heat transport into the Arctic in the PAMIP experiments. *Geophys. Res. Lett.* **48**, e2020GL089990 (2021).
41. Xu, M. et al. Important role of stratosphere-troposphere coupling in the Arctic mid-to-upper tropospheric warming in response to sea-ice loss. *npj Clim. Atmos. Sci.* **6**, 9 (2023).
42. Zhang, J. et al. Persistent shift of the Arctic polar vortex towards the Eurasian continent in recent decades. *Nat. Clim. Change* **6**, 1094–1099 (2016).
43. Cohen, J. et al. Linking Arctic variability and change with extreme winter weather in the United States. *Science* **373**, 1116–1121 (2021).
44. Zou, C. et al. Contrasting physical mechanisms linking stratospheric polar vortex stretching events to cold Eurasia between autumn and late winter. *Clim. Dyn.* **62**, 2399–2417 (2024).
45. Zou, C. & Zhang, R. Arctic sea ice loss modulates the surface impact of autumn stratospheric polar vortex stretching events. *Geophys. Res. Lett.* **51**, e2023GL107221 (2024).
46. Siew, P. Y. F. et al. Intermittency of Arctic–mid-latitude teleconnections: stratospheric pathway between autumn sea ice and the winter North Atlantic Oscillation. *Weather Clim. Dyn.* **1**, 261–275 (2020).
47. Xu, M. et al. Impact of sea ice reduction in the Barents and Kara Seas on the variation of the East Asian trough in late winter. *J. Clim.* **34**, 1081–1097 (2021a).
48. He, S. et al. Eurasian cooling linked to the vertical distribution of Arctic warming. *Geophys. Res. Lett.* **47**, e2020GL087212 (2020).
49. Labe, Z., Peings, Y. & Magnusdottir, G. Warm Arctic, cold Siberia pattern: Role of full Arctic amplification versus sea ice loss alone. *Geophys. Res. Lett.* **47**, e2020GL088583 (2020).
50. Sellevold, R., Sobolowski, S. & Li, C. Investigating possible Arctic–midlatitude teleconnections in a linear framework. *J. Clim.* **29**, 7329–7343 (2016).
51. Geen, R. et al. An explanation for the metric dependence of the midlatitude jet-waviness change in response to polar warming. *Geophys. Res. Lett.* **50**, e2023GL105132 (2023).
52. Mudhar, R. et al. Exploring mechanisms for model-dependency of the stratospheric response to Arctic warming. *J. Geophys. Res. Atmos.* **129**, e2023JD040416 (2024).
53. Xu, X. et al. Contributors to linkage between Arctic warming and East Asian winter climate. *Clim. Dyn.* **57**, 2543–2555 (2021).
54. Zhang, R., Zhang, R. & Dai, G. Intraseasonal contributions of Arctic sea-ice loss and Pacific decadal oscillation to a century cold event during early 2020/21 winter. *Clim. Dyn.* **58**, 741–758 (2022).
55. Takaya, K. & Nakamura, H. A formulation of a phase-independent wave-activity flux for stationary and migratory quasigeostrophic eddies on a zonally varying basic flow. *J. Atmos. Sci.* **58**, 608–627 (2001).
56. Cohen, J., Saito, K. & Entekhabi, D. The role of the Siberian high in Northern Hemisphere climate variability. *Geophys. Res. Lett.* **28**, 299–302 (2001).
57. Wu, B. Y. et al. Effects of autumn–winter Arctic sea ice on winter Siberian High. *Chin. Bull.* **56**, 3220–3228 (2011).
58. Tang, Q. et al. Cold winter extremes in northern continents linked to Arctic sea ice loss. *Environ. Res. Lett.* **8**, 014036 (2013).
59. Huang, R. et al. Characteristics, processes, and causes of the spatio-temporal variabilities of the East Asian monsoon system. *Adv. Atmos. Sci.* **29**, 910–942 (2012).
60. Chuan, F. & Wu, B. Enhancement of winter Arctic warming by the Siberian high over the past decade. *Atmos. Ocean Sci. Lett.* **8**, 257–263 (2015).
61. England, M. R., Eisenman, I. & Wagner, T. J. W. Spurious climate impacts in coupled sea ice loss simulations. *J. Clim.* **35**, 7401–7411 (2022).
62. Fraser-Leach, L., Kushner, P. & Audette, A. Correcting for artificial heat in coupled sea ice perturbation experiments. *Environ. Res. Clim.* **3**, 015003 (2023).
63. Lewis, N. T. et al. Assessing the spurious impacts of ice-constraining methods on the climate response to sea-ice loss using an Idealised aquaplanet GCM. *J. Clim.* **37**, 6729–6750 (2024).
64. Hersbach, H. et al. The ERA5 global reanalysis. *Q. J. R. Meteorol. Soc.* **146**, 1999–2049 (2020).
65. Zhang, J. & Rothrock, D. A. Modeling global sea ice with a thickness and enthalpy distribution model in generalized curvilinear coordinates. *Mon. Weather Rev.* **131**, 845–861 (2003).
66. Andrews, D. G., Holton, J. R. & Leovy, C. B. *Middle Atmosphere Dynamics* Vol. 489 (California Academic Press Inc., 1987).
67. Smith, K. L. et al. The specified chemistry whole atmosphere community climate model (SC-WACCM). *J. Adv. Model. Earth Syst.* **6**, 883–901 (2014).
68. Bailey, D. et al. *Community Ice Code (CICE) User's Guide Version 4.0 Released with CCSM 4.0*. Technical report (Los Alamos National Library, 2011).
69. Smith, R. et al. The Parallel Ocean Program (POP) Reference Manual Ocean Component of the Community Climate System Model (CCSM) and Community Earth System Model (CESM). *REP. LAUR-01853* **141**, 1–140 (2010).
70. Rayner, N. A. A. Global analyses of sea surface temperature, sea ice, and night marine air temperature since the late nineteenth century. *J. Geophys. Res. Atmos.* **108**, D14 (2003).
71. Gilleland, E. Bootstrap methods for statistical inference. Part I: Comparative forecast verification for continuous variables. *J. Atmos. Ocean. Technol.* **37**, 2117–2134 (2020).
72. Audette, A. Simple hybrid sea ice nudging method for improving control over partitioning of sea ice concentration and thickness. Zenodo, <https://doi.org/10.5281/zenodo.7072571> (2022).

Acknowledgements

This research was supported by the Gansu Provincial Science and Technology Program (22ZD6FA005), the National Natural Science Foundation of China (42401170, 42130601), the Gansu Provincial Science and Technology Funding (24JRRA115) and the National Postdoctoral Researcher Program (GZC20232950). The authors thank the help from Dr. Mark England on the sea-ice nudging technique. The authors also thank the high-performance computing support from Supercomputing Center of Lanzhou University, the UK's collaborative data analysis environment (JASMIN, <https://www.jasmin.ac.uk>) and School of Atmospheric Science of Sun Yat-sen University.

Author contributions

M.X., S.C.K., and W.S.T. designed the project. M.X. and A.A. performed model experiments and data analysis. J.A.S. interpreted the data and results and revised the manuscript. J.K.Z., H.Y., and H.Z. calculated some diagnostics used in this study. All authors contributed to the writing of the paper.

Competing interests

The authors declare no competing interests.

Additional information

Supplementary information The online version contains supplementary material available at <https://doi.org/10.1038/s41612-025-01211-9>.

Correspondence and requests for materials should be addressed to Shichang Kang.

Reprints and permissions information is available at <http://www.nature.com/reprints>

Publisher's note Springer Nature remains neutral with regard to jurisdictional claims in published maps and institutional affiliations.

Open Access This article is licensed under a Creative Commons Attribution-NonCommercial-NoDerivatives 4.0 International License, which permits any non-commercial use, sharing, distribution and reproduction in any medium or format, as long as you give appropriate credit to the original author(s) and the source, provide a link to the Creative Commons licence, and indicate if you modified the licensed material. You do not have permission under this licence to share adapted material derived from this article or parts of it. The images or other third party material in this article are included in the article's Creative Commons licence, unless indicated otherwise in a credit line to the material. If material is not included in the article's Creative Commons licence and your intended use is not permitted by statutory regulation or exceeds the permitted use, you will need to obtain permission directly from the copyright holder. To view a copy of this licence, visit <http://creativecommons.org/licenses/by-nc-nd/4.0/>.

© The Author(s) 2025